

Article

# Performance Enhancement of Roof-Mounted Photovoltaic System: Artificial Neural Network Optimization of Ground Coverage Ratio

Ali S. Alghamdi 

Department of Electrical Engineering, College of Engineering, Majmaah University, Majmaah 11952, Saudi Arabia; aalghamdi@mu.edu.sa

**Abstract:** Buildings in hot climate areas are responsible for high energy consumption due to high cooling load requirements which lead to high greenhouse gas emissions. In order to curtail the stress on the national grid and reduce the atmospheric emissions, it is of prime importance that buildings produce their own onsite electrical energy using renewable energy resources. Photovoltaic (PV) technology is the most favorable option to produce onsite electricity in buildings. Installation of PV modules on the roof of the buildings in hot climate areas has a twofold advantage of acting as a shading device for the roof to reduce the cooling energy requirement of the building while producing electricity. A high ground coverage ratio provides more shading, but it decreases the efficiency of the PV system because of self-shading of the PV modules. The aim of this paper was to determine the optimal value of the ground coverage ratio which gives maximum overall performance of the roof-mounted PV system by considering roof surface shading and self-shading of the parallel PV modules. An unsupervised artificial neural network approach was implemented for Net levelized cost of energy (*Net-LCOE*) optimization. The gradient decent learning rule was used to optimize the network connection weights and the optimal ground coverage ratio was obtained. The proposed optimized roof-mounted PV system was shown to have many distinct performance advantages over a typical ground-mounted PV configuration such as 2.9% better capacity factor, 15.9% more energy yield, 40% high performance ratio, 14.4% less LCOE, and 18.6% shorter payback period. The research work validates that a roof-mounted PV system in a hot climate area is a very useful option to meet the energy demand of buildings.



**Citation:** Alghamdi, A.S. Performance Enhancement of Roof-Mounted Photovoltaic System: Artificial Neural Network Optimization of Ground Coverage Ratio. *Energies* **2021**, *14*, 1537. <https://doi.org/10.3390/en14061537>

Academic Editor:  
Alessandro Bianchini

Received: 16 February 2021  
Accepted: 6 March 2021  
Published: 10 March 2021

**Publisher's Note:** MDPI stays neutral with regard to jurisdictional claims in published maps and institutional affiliations.



**Copyright:** © 2021 by the author. Licensee MDPI, Basel, Switzerland. This article is an open access article distributed under the terms and conditions of the Creative Commons Attribution (CC BY) license (<https://creativecommons.org/licenses/by/4.0/>).

**Keywords:** roof-mounted PV; shading; artificial neural network; buildings; optimization; levelized cost of energy; payback period

## 1. Introduction

The population in cities is increasing at a rapid rate and people spend most of their time inside the buildings [1]. Buildings contribute 30% in greenhouse gases (GHG) emissions by consuming 20% to 40% of total generated electricity [2,3]. In order to overcome the high electricity consumption and high GHG emissions of buildings, some countries have introduced building laws to ensure that buildings are energy efficient, emit less GHG, and generate their own onsite electricity [4]. The European Union 2020 directive about building laws says that by 2020, buildings should consume 20% less electricity, emit 20% less GHG, and generate 20% onsite energy by using renewable resources [5]. The electricity consumption of buildings in the European Union countries is 40% of the total electricity requirements [6] while this share is 80% in Saudi Arabian buildings [7]. Although the country is committed to include a large share of solar energy-based power generation in its national grid [8], unfortunately, no attention has been given to transform buildings from just users of energy to producers of energy [9]. Several countries in Europe have defined national guidelines to include renewable energy resources in buildings [10] but no proper guidelines or framework has yet been developed in this regard in Saudi Arabia.

Photovoltaic is a very attractive option to generate onsite electricity in urban areas [11,12]. This solar energy technology produces electricity by direct conversion of sunlight to DC power [13]. Since this technology has no GHG emissions during its operation, it is therefore environmentally friendly [14–16]. There has been a significant drop in the prices of *PV* panels in recent years [17] and a cost drop of 80% has been seen in the last decade [18]. The roof of a building is the most feasible place for *PV* installations in urban areas [19]. The excess energy, during peak solar irradiance time, can be sold to the grid by employing a net-metering system [12]. Buildings receive heat from windows, roof, and facades. The density of buildings in the urban environment is generally very high which provides shading for windows and walls. However, the roofs of buildings are directly exposed to sun [20]. The solar radiations heat up the roof and then the roof transfers the heat inside the building through conduction and convection processes. It acts as a major interface between the interior of the building and the outside atmosphere. The color of the roofs is generally dark and therefore, they absorb the main chunk of thermal energy of solar radiations [21]. Hence, the temperature of the interior of the building increases. Therefore, the energy demand of the buildings is very high in areas with a hot climate [22]. There is a steady increase in the building energy consumption rate, both in cold and hot regions across the world and the office buildings have the highest energy demand with 17% share in the global energy requirements of the world [23].

The electrical energy consumption of the gulf countries is very high during the summer solstice and Saudi Arabia has the highest summer season electricity demand in this region [24]. The summer season electrical load of Saudi Arabia has a rapid growth due to the very hot climate and the peak electrical load during summer is very high compared to the peak load in the winter season [25]. The cooling energy requirement of buildings is the major cause of the high load during summer. Global warming will further aggravate the situation due to the overall temperature rise worldwide [26]. The high energy requirements of buildings in Saudi Arabia during the hot summer can be fulfilled by installing *PV* panels on the buildings. The other advantage of *PV* technology is that its energy output is high during the daytime which could be very useful for office building with working hours in the daytime. The *PV* panels can be integrated in facades and windows or can be placed on the roof of buildings. The integration *PV* modules in facades and windows reduces their efficiency because such *PV* modules are mostly vertical and the optimal tilt angle and orientation to receive maximum solar irradiance is not available [27]. On the other hand, *PV* modules installed on the roof, block the direct connection of sun rays with the roof. Therefore, the roof is the most favorable option to install a *PV* system in buildings [19] and roof-mounted *PVs* could act as shading devices particularly in office buildings with daytime working hours [28].

Mandalaki et al. [29] investigated the performance of 13 different shading devices having *PV* as their integral part. Their performance was evaluated for two different locations, in China and Athens, for a small office room with one occupant. The authors in another study presented a method of calculation of roof surface area for large-scale *PV* installations in a community [30]. They also studied the losses due to shading from surrounding buildings and trees, but they did not consider the self-shading of the tilted *PV* arrays. Yadav et al. [31] evaluated a 5 kW roof-mounted *PV* system based on various performance criteria such as energy yield, capacity factor, energy output, and efficiency of array. Another study tested the performance of a 200 kW roof-integrated *PV* setup in India by evaluating capacity factor, performance ratio, and overall efficiency [32]. Shukla et al. [33] conducted an in-depth techno-economic analysis of a 110 kW rooftop *PV* system for India without taking into account the shading advantage of *PVs*. Awan et al. [34] performed a parametric optimization of rooftop and ground-mounted *PV* systems and compared the performance of the two optimized systems. Dondariya et al. [35] investigated a *PV* system of 6.4 kW capacity installed on the roof of a building in India but the shading advantage and self-shading effect of the *PV* modules was not included in their research work. Akpolat

et al. [36] analyzed a roof integrated *PV* setup for Marmara University's staff building in Turkey. Their roof integrated *PV* system achieved a 73% performance ratio.

The literature review proves that the use of *PV* technology for energy generation in buildings is very important and is being investigated by many researchers across the world. Many researchers have analyzed the performance of roof-mounted *PV* systems but most of them did not consider the self-shading and cooling load saving benefits of a roof-mounted *PV* system. Several studies performed a parametric optimization of rooftop *PV* systems. This research work investigated the detailed performance of a roof-mounted *PV* system by optimizing the ground coverage ratio of the *PV* system on the roof while considering the self-shading and roof shading of the *PV* modules. An artificial neural network incorporating a gradient decent learning algorithm was applied to find the optimal value of ground coverage ratio of the proposed roof-mounted *PV* system.

## 2. Methodology

In order to optimize the ground coverage ratio of a rooftop *PV* system while taking into account the self-shading of parallel *PV* arrays and rooftop surface shading, the following methodological approach was adopted.

- The solar resource data at the proposed location was obtained from the monitoring station near the administration building of Majmaah University (ABMU).
- The layout of the rooftop *PV* system on the roof of the ABMU was designed in Helioscope software. This software gives a freedom to the user to avoid any obstacles on the given surface and to determine the exact available area of the roof which can be used for *PV* installation. Due to its design-integration approach, it helps to model the *PV* system based on the physical design.
- The model of the building was simulated in EnergyPlus software to determine the cooling load requirement and roof surface temperatures under different shading scenarios
- The temperature of roof surface and required cooling load of the ABMU was determined by simulating the building in EnergyPlus software.
- The energy production calculations of the various arrangement of the *PV* system with different ground coverage ratios were carried out in System Advisor Model.
- The cost and energy analysis to determine the optimal value of ground coverage ratio was performed based on incorporating the savings of energy in terms of reduced cooling load due to shading of the roof provided by rooftop *PV* panels.
- The optimal value of ground coverage ratio was determined by using an unsupervised neural network based on the gradient descent learning rule.

## 3. Analysis of the Proposed Location

Saudi Arabia is part of the solar belt region and it has very rich solar resource. The government has a policy to explore this massive renewable energy resource. According to its vision 2030, the country has a plan to install 9.5 GW capacity of renewable energy technologies including solar technologies [8]. In this regard, Saudi Arabia has installed renewable energy resource monitoring stations at 46 different sites throughout the country. One of such monitoring stations is located in Majmaah University. The main ABMU was selected for the installation of the roof-mounted *PV* system. The data of solar resource at the proposed location was obtained from the monitoring station near the ABMU and is listed in Table 1. The Saudi Arabian climate is extremely hot; hence, the electrical load of the building rises during the summer season because of the high cooling load demand of the building. Table 1 illustrates that *GHI* (Global Horizontal Irradiance) at the proposed site is high during the summer solstice which shows that the *GHI* profile follows the load pattern at the project location. The average value of *GHI* is 6.04 kWh/m<sup>2</sup>/day and the maximum average *GHI* of 8.45 kWh/m<sup>2</sup>/day is seen in June while the minimum value of 3.9 kWh/m<sup>2</sup>/day appears in December.

**Table 1.** Solar resource data for year 2019 [25].

Months	Parameter	<i>GHI</i>	Average Temperature (°C)	Daytime Average Temperature (°C)
January		4.35	13.3	14.9
February		5.45	16.3	18.1
March		5.92	21.5	23.4
April		7.36	24.8	26.3
May		8.06	31.7	33.3
June		8.45	34.7	36.8
July		8.32	36.6	38.4
August		7.42	36.4	38.2
September		6.83	32.9	34.9
October		5.49	26.1	27.9
November		4.24	19.1	21
December		3.9	13.2	14.8

#### 4. Design of Rooftop PV System

The electrical energy produced by a *PV* system depends on four parameters which are the solar irradiance striking the plane of the *PV* array, ground reflectance, ambient temperature that affects the *PV* cell temperature, and derating factor. The incident solar irradiance is the most dominant factor for *PV* performance at a particular site. The electrical output per meter square of *PV* is given by [25]

$$P = X_{PV} F_{PV} \left( \frac{G}{G_{STC}} \right) [1 + \alpha_P (T_{cell} - T_{cell\_STC})] \quad (1)$$

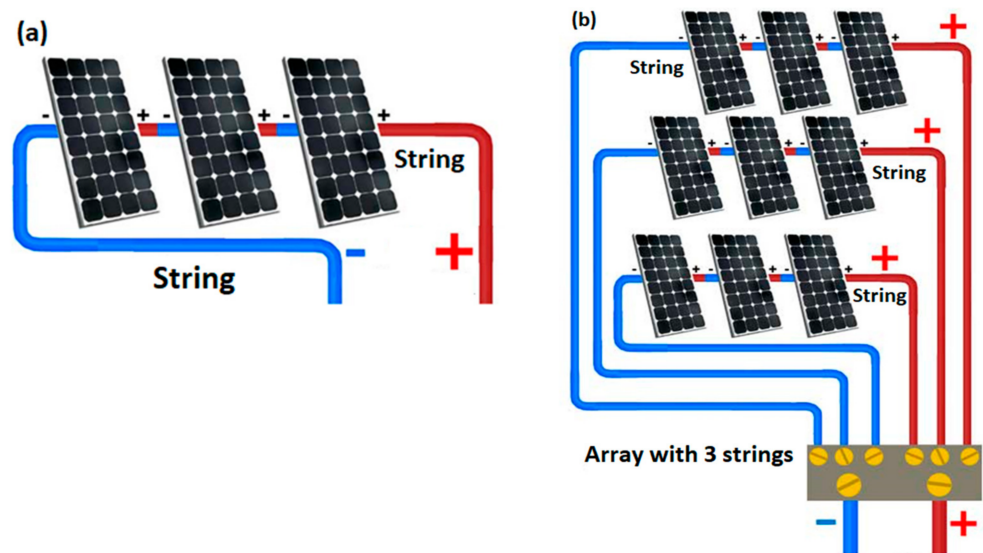
where, *STC* is standard test conditions,  $F_{PV}$  is derating factor of *PV*,  $X_{PV}$  is *PV* output at *STC*,  $G$  is plane of array solar radiations,  $G_{STC}$  is solar radiation at *STC*,  $T_{cell}$  is *PV* cell temperature,  $T_{cell\_STC}$  is *PV* cell temperature at *STC*, and  $\alpha_P$  is temperature coefficient of power.

The output power of the *PV* system is directly proportional to the solar irradiance on the *PV* array. Dust and shading affect the output of the *PV* system and which is indicated by the derating factor of *PV*. Said [37] measured the average annual efficiency degradation of 7% for *PV* panels in the Riyadh region of Saudi Arabia. Baras et al. [38] measured the performance degradation of *PV* due to dust and soiling in the central part of Saudi Arabia and their results shown approximately 2% losses during the least dustiest month (July) versus approximately 16% losses during the dustiest month (April). Based on the information available in the literature an average performance derating factor of 10% over the whole year is considered for the proposed *PV* system. The influence of ground reflectance on the *PV* output is relatively modest. It represents the percentage of solar radiations reflected from the surface on which *PV* panels are installed. The cell temperature of the *PV* is higher than the ambient temperature because the *PV* modules are dark in color. The  $\alpha_P$  is a negative number therefore each degree rise in cell temperature decreases the output of the *PV* system by a small fraction. Monocrystalline *PV* panels are used for the proposed system because of their better efficiency compared to polycrystalline technology. The SUP ERPOWER CS6K-300 MS *PV* panel was used in this research work. It is a PERC monocrystalline *PV* panel. It offers better performance during the low irradiance period in the morning, evening and overcast conditions. The detailed specifications of the *PV* module are listed in Table 2.

**Table 2.** Specifications of the *PV* modules.

Description	Specification
Power rating	300 W
Efficiency	18.33%
Operating current (optimum)	9.24 A
Current (Open circuit)	9.83 A
Operating voltage (optimum)	32.5 V
Voltage (Open circuit)	39.7 V
Operating temperature	$-40\text{ }^{\circ}\text{C} \pm 85\text{ }^{\circ}\text{C}$
Nominal operating cell temperature	$45 \pm 2\text{ }^{\circ}\text{C}$
Temperature coefficient of power	$-0.39/\text{ }^{\circ}\text{C}$
Lifetime	25 years

The series connection of many *PV* modules creates a *PV* string (Figure 1a). These strings are placed in parallel rows and are connected in series and parallel to obtain a required voltage and current to form a *PV* array (Figure 1b). The total roof area for the proposed rooftop *PV* system is 2349 m<sup>2</sup>. There are some other installations of cooling system and water tanks existing on the roof; hence, the available area of the roof for *PV* installation is 1440 m<sup>2</sup>. The strings of *PV* modules are placed on the roof in parallel rows at a tilt angle of 25° to increase the plane of array solar irradiance. The tilt angle for the proposed *PV* system is selected close to the latitude of the location (25.86). The tilted *PV* arrays cause self-shedding of *PV* modules which affects their performance. The *PV* system is designed and evaluated for various ground coverage ratios. The layout of the *PV* system for a ground coverage ratio of 0.6 is shown in Figure 2. The available area of the roof of ABMU is limited therefore the total capacity of the *PV* system decreases as the ground coverage ratios decreases.

**Figure 1.** (a) *PV* string (b) *PV* arrays.

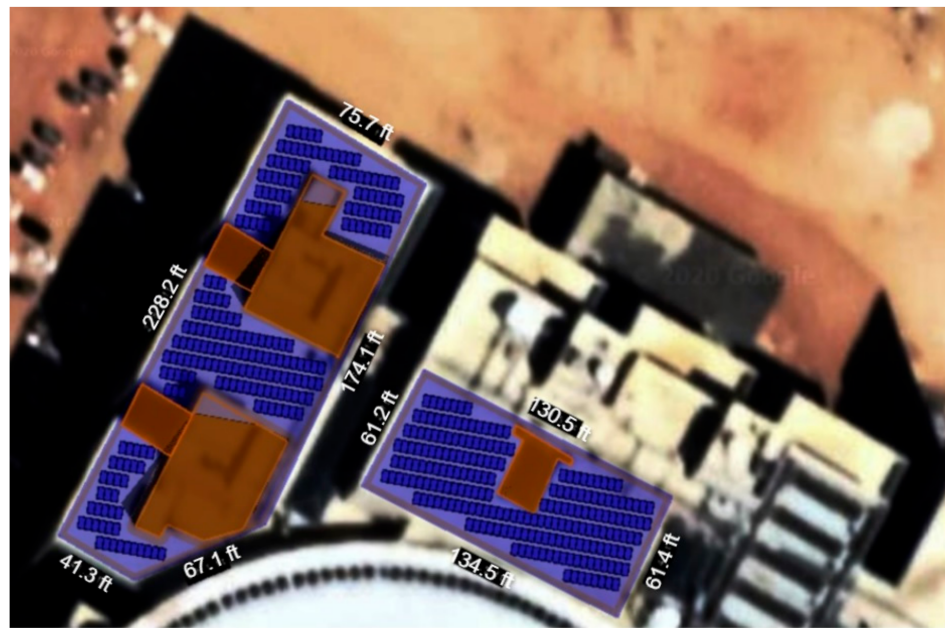


Figure 2. PV system layout on the roof of ABMU.

### 5. Building Simulation and Analysis

The ABMU is located at  $25.861^{\circ}$  N and  $45.421^{\circ}$  E in the Riyadh region, Saudi Arabia. The building has three stories, but only the upper story is used for the analysis because the heat of the sun rays directly affects the upper story of the building. As working hours of the ABMU are during the daytime, the peak load therefore appears during the daytime which means PV could be an effective alternative choice for supplying the load demand of the building because the PV energy production hours match with the working hours of the building. The hourly average monthly electrical load profile of the ABMU is shown in Figure 3. The electricity consumption of the building is low from November to March, but the electricity consumption is very high during the summer months especially from May to September. This high electricity consumption is due to the very high temperature during these hot summer months which leads to high cooling load requirement of the building. The roof of the building is one of the major sources of absorbing direct sun radiations which causes an increase in the air conditioning load. The installation of PV panels on the roof could provide a very useful shading advantage by blocking the direct sun rays.

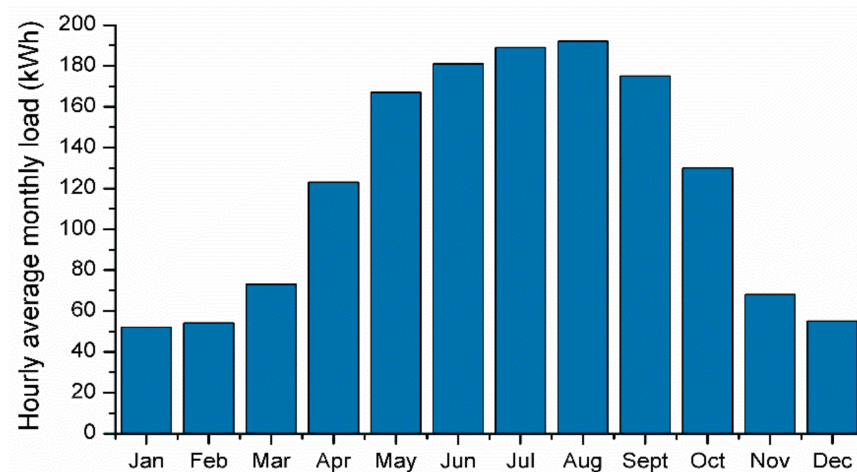


Figure 3. Hourly average monthly electrical load profile of ABMU.

For calculating the cooling energy demand of the ABMU for various configurations of roof-mounted PV at different ground coverage ratios, the simulation of the building was carried out using Energyplus software. In order to find the roof temperatures and heat transfer into the building, the weather data file of GHI, DNI (Direct Normal Irradiance), DHI (Diffuse Horizontal Irradiance), temperature, wind speed, humidity etc. was used as input to the software. The steps to setup the building parameters in EnergyPlus are listed below:

- The population density of the top floor of ABMU is 5 people per100 m<sup>2</sup>
- The cooling and heating loads' thermostat settings are set at 25 °C and 20 °C respectively.
- Electrical equipment load power density is set at 11 W/m<sup>2</sup>
- Lighting load power density is set at 11 W/m<sup>2</sup>
- Characteristics (Roof exterior)
  - Out-side layer—Concrete 100 mm M11 (R-value 0.22 K.m<sup>2</sup>/W and Specific heat 850 J/kg K)
  - Layer-2—Airspace resistance of ceiling (R-value 0.22 K.m<sup>2</sup>/W)
  - Layer-3—Acoustic tile F16 (Specific heat 580 J/kg K)
  - Solar reflectance (0.3)
- Characteristics (Roof interior)
  - Outside layer—Concrete 100 mm M11
  - Layer-2—Airspace resistance of ceiling
  - Layer-3—Acoustic tile F16
- Set the lighting schedule
- Set the building occupancy schedule
- Characteristics (Windows)
  - Interior layer (clear, 3 mm)
  - Exterior layer (clear, 3 mm)
  - Air gap (13 mm)

Only the top floor of the ABMU is considered for the analysis because shading of the rooftop-mounted PV system only affects the cooling load of the top floor of the building. The heat flux balance equation of the roof of the building is

$$q_{Roof} - q_{SW} - q_{LW} - q_{conv} = 0 \quad (2)$$

where,  $q_{Roof}$  represents total heat flux transfer into the roof,  $q_{SW}$  is the shortwave solar radiation heat flux which comprises diffused and direct radiations received by the outer surface of roof. The  $q_{LW}$  is the part of the heat flux from longwave radiation exchange with the surrounding high-rise buildings, air, and sky. The  $q_{conv}$  is convection heat flux by air. The flux part by convection is modelled as

$$q_{conv} = h_c(T_r - T_a) \quad (3)$$

where,  $T_r$  is the temperature of the roof surface,  $T_a$  is air temperature, and  $h_c$  is the convection coefficient. The shortwave solar radiation heat flux is the accumulative effect of direct and diffuse components of the solar radiations reaching the surface of the roof. It is given by [39]

$$q_{SW} = (1 - \alpha_r)GHI \quad (4)$$

where,  $\alpha_r$  denotes the surface albedo of roof. When roof is shaded with PVs then the GHI is reduced to diffuse solar radiations (*Dif*)

$$q_{SW} = (1 - \alpha_r)Dif \quad (5)$$

The surfaces of different bodies exchange heat flux between each other depending on their temperature difference. The surfaces with higher temperature radiate heat while this

heat is absorbed by the surfaces with lower temperature depending on the respective view factors. The longwave heat flux component of the heat flux balance equation represents this heat flux exchange. The longwave heat flux component for the rooftop surface is defined as [39]

$$q_{LW} = q_{air} + q_{sky} \quad (6)$$

where,  $q_{sky}$  and  $q_{air}$  are heat fluxes due to exchange of radiation from sky and air. These heat flux components are dictated by the temperature difference of the bodies. Using the Stefan–Boltzmann law along with the respective view factors of sky and air, the longwave heat flux expression further expands as [39,40]

$$q_{LW} = F_{air}\varepsilon\sigma(T_a^4 - T_r^4) + F_{sky}\varepsilon\sigma(T_{sky}^4 - T_r^4) \quad (7)$$

where  $F_{sky}$  is the roof surface view factor to sky,  $F_{air}$  is the roof surface view factor to air,  $T_{sky}$  is sky temperature,  $\varepsilon$  is emissivity,  $\sigma$  is the Stefan–Boltzmann constant. When PV panels are placed on the surface of the roof then the roof view factors are modified. The PV panels also radiate heat from the back side; Therefore, the longwave radiation flux expression for a roof with rooftop PVs can be modified as [39,40]

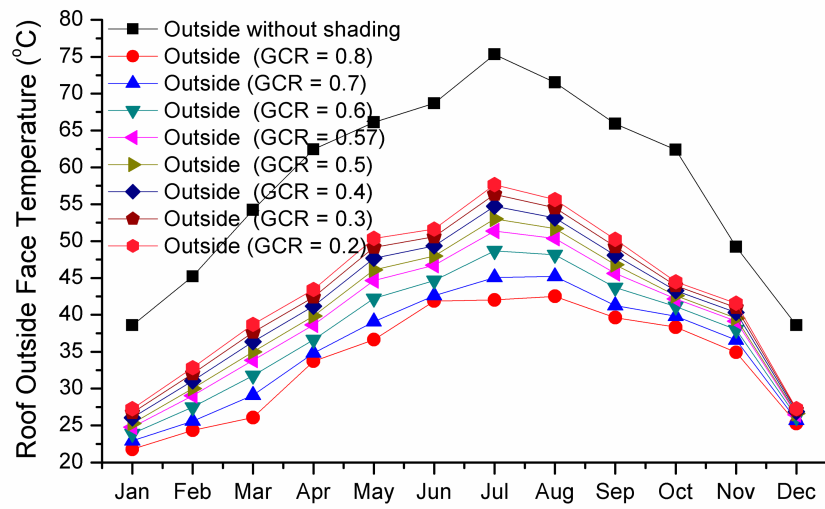
$$q_{LW} = \varepsilon\sigma F_{air}(T_a^4 - T_r^4) + \varepsilon\sigma F_{sky}(T_{sky}^4 - T_r^4) + \varepsilon\sigma F_{PV}(T_{PV\_b}^4 - T_r^4) \quad (8)$$

where,  $F_{PV}$  is the roof surface view factor to PV back surface,  $T_{PV\_b}$  is temperature of back surface of the PV. By adding the expressions of convection, shortwave and longwave heat fluxes in the heat flux balance equation gives the expression of the total heat flux entering the roof as

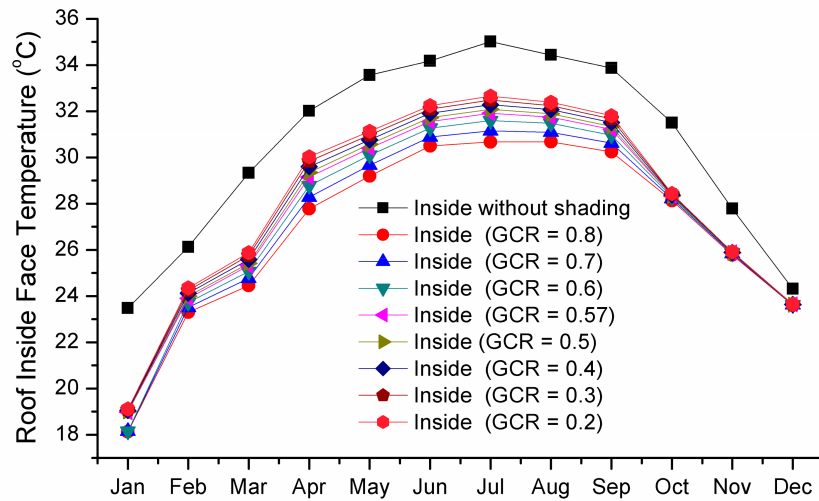
$$q_{Roof} = h_c(T_r - T_a) + (1 - \alpha_r)Dif + F_{air}\varepsilon\sigma(T_a^4 - T_r^4) + F_{sky}\varepsilon\sigma(T_{sky}^4 - T_r^4) + \varepsilon\sigma F_{PV}(T_{PV\_b}^4 - T_r^4) \quad (9)$$

In order to evaluate the effect of the rooftop PV system, the ABMU is first simulated without PV panels on the roof and then the simulation is carried out for different ground coverage ratios of PV arrays. The results of the simulation illustrate that the temperature of the roof surface increases up to more than 70 °C during the summer solstice. When the PV modules are installed on the rooftop, they provide partial shading of the roof and as a result the percentage of solar radiations directly hitting the roof surface reduces. The portion of the roof covered with PV modules only receives heat flux through diffused radiation. As a result, the roof temperature reduces and less heat is transferred inside the building from the roof; therefore, the cooling energy required by the building reduces. The maximum roof temperatures for different ground coverage ratio values for each month are shown in Figure 4. The temperatures of both the interior and exterior surface of the roof decreases by increasing the ground coverage ratio, which means the building's cooling load will decrease.

The results of the ABMU simulation show that the top floor of the proposed building will consume less energy for cooling purposes when PV modules are installed on the roof. The actual consumption of cooling energy and percentage savings in the cooling load at different ground coverage ratio values are depicted in Figure 5.



(a)



(b)

Figure 4. Maximum roof temperatures for different ground coverage ratio values. (a) Outside face, (b) Inside face.

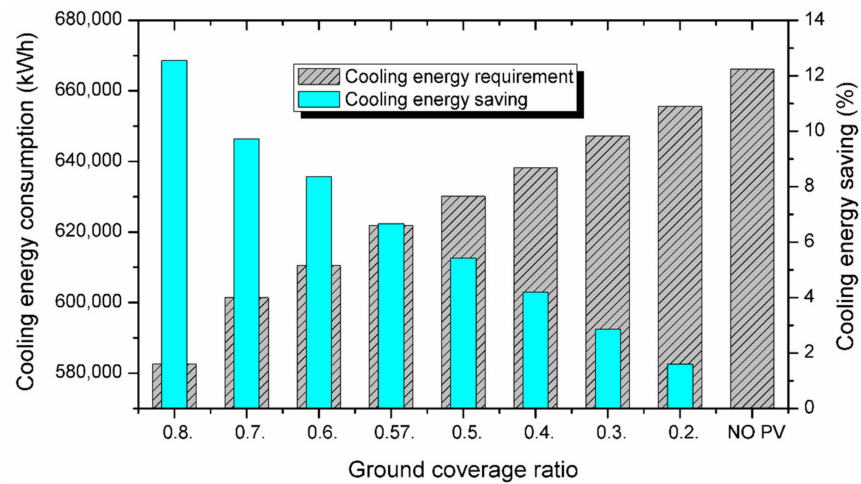


Figure 5. Cooling energy requirement and percentage savings at different ground coverage ratio values.

## 6. Optimization of PV Systems

In order to increase the intensity of solar irradiance on the plane of the PV array, the PV modules are installed on the roof at a tilt angle. These tilted modules cause self-shading between the PV modules placed in parallel rows. As a result, the efficiency of the PV system decreases. This can be avoided by decreasing the ground coverage ratio of PV modules which will increase the distance between the parallel modules. However, this reduced ground coverage ratio results in more area of the roof surface exposed to sun rays. Therefore, more heat flux enters the building from the roof and the cooling energy load increases. Hence, it is of prime importance to determine an optimal value of ground coverage ratio. The ground coverage ratio is optimized while the objective is to minimize the LCOE (Levelized Cost of Energy). The LCOE is calculated by dividing the annualized cost of the PV system by its annual energy production and is expressed as [41]

$$LCOE = \frac{C_{AN}}{E_{PV}} \quad (10)$$

where  $C_{AN}$  is the annualized cost and  $E_{PV}$  is the annual energy production of the PV system and it is given by the following relation [41]

$$E_{PV} = A_{PV} \sum_{n=1}^{8760} P(n) \quad (11)$$

where  $n$  is the hour number,  $P(n)$  is the electrical output of PV in hours  $n$  which is given by Equation (1), and  $A_{PV}$  is the active area of the PV array.

The energy yield in the case of the roof-mounted PV system is the Net-energy yield and it is the sum of the PV electrical energy yield and the cooling energy saving yield. Similarly, LCOE is the Net-LCOE which is obtained by adding the cooling energy saving advantage (Figure 5) of roof-mounted PVs. The Net-LCOE of the roof-mounted PV system is given by adding the cooling energy savings in the denominator of Equation (10)

$$Net - LCOE = \frac{C_{AN}}{E_{PV} + E_{sav}} \quad (12)$$

where  $E_{sav}$  is the annual saving in cooling energy by installing roof-mounted PVs on the building. The economic parameters for calculating the Net-LCOE are listed in Table 3.

The total annualized cost is calculated as [42]

$$C_{AN} = C_{TPV} \times CRF \quad (13)$$

where,  $C_{TPV}$  is the net present value of all the costs and  $CRF$  is the capital recovery factor which is expressed as [43]

$$CRF = \frac{r(1+r)^N}{(1+r)^N - 1} \quad (14)$$

where  $r$  is the interest rate and  $N$  is the project duration (25 years). The net present value of all the costs is calculated as

$$C_{TPV} = CC + C_{O\&M\_NPV} + C_{Rep\_NPV} - C_{G\_NPV} \quad (15)$$

where,  $CC$  is the capital cost,  $C_{Rep\_NPV}$  is the present value of the replacement cost of equipment,  $C_{O\&M\_NPV}$  is the present value of the operation and maintenance cost, and  $C_{G\_NPV}$  is the present worth of cooling load saving in terms of grid electricity price. The electricity price of a government building in Saudi Arabia is 8.5 ¢/kWh [44].

**Table 3.** Roof-mounted PV system's economic parameters [45].

Parameter	Cost
Inverter	130 US\$/kW <sub>dc</sub>
PV module	450 US\$/kW <sub>dc</sub>
Balance of system	100 US\$/kW <sub>dc</sub>
Labor	200 US\$/kW <sub>dc</sub>
Sales tax	5.0%
Operation and maintenance cost	20 US\$/kW/year

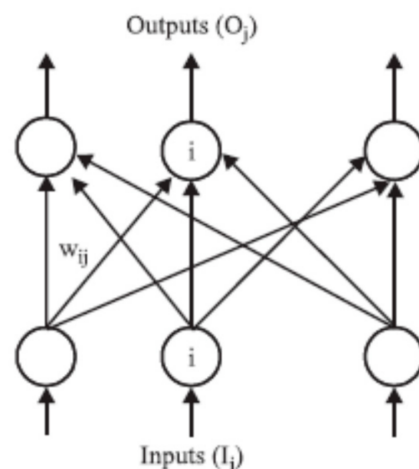
The final form of the *Net-LCOE* optimization objective function is

$$\text{Minimize } F(x) = \frac{C_{AN}}{E_{PV} + E_{sav}} \quad (16)$$

subject to the optimization constraint of the ground coverage ratio

$$0.1 \leq x \leq 0.9 \quad (17)$$

An unsupervised neural network incorporating the gradient decent learning algorithm was developed with the present problem based on the minimization of energy function, here the energy function is in terms of the objective and constraints. The two-layer network has the number of outputs equal to the number of design variables to be determined. The connection of weights between the input and output layers are obtained by minimization of the formulated energy function. The architecture of the proposed two-layer network is shown in Figure 6.

**Figure 6.** Two-layer neural network.

The network learning is based on the following rules:  
Change in weights is found by

$$\Delta w_{ij} = -\eta I_i \nabla E \quad (18)$$

where  $I_i$  is the input to the  $i$ th node of input layer;  $\nabla E$  is the gradient of the energy function  $E$ , and  $\eta$  is the learning rate (whose values lies between 0 and 1). Initially, a set of random weights are assigned, and outputs are computed according to

$$O_j = \eta \sum_{i=1}^n I_i w_{ij} \quad (19)$$

In the present optimization methodology, the energy function is represented by

$$E = F(X) + K \sum_{i=1}^n P[r_i(X)] \quad (20)$$

where,  $F(X)$  is objective function (*Net-LCOE*) to be minimized and  $K$  is the penalty constant which is preferably a large number;  $P[r_i(X)]$  is a penalty function which may be taken as  $r^2$  which is the residual of the constraint (ground coverage ratio) violation.

It can be seen from the above equations that the energy function has a set of connection weights as the only variables. The process of energy function minimization is repeated several times. In one cycle, the network takes both random inputs and connection weights, and computes the energy function and at the end of the cycle the connection weights are updated based on a gradient descent learning rule. This is repeated several times until, the energy reduces to a minimum and the weight set stabilizes. The corresponding outputs give the optimum parameter-set of the objective function. All the constraints are properly handled at every point and, if any deviations are observed they are given as a penalty. In the selection of inputs of the network, there is a flexibility that one can select a fixed set of inputs for every problem since the objective and constraints are defined in the energy function. The network took 20,000 cycles, until the energy was minimized, and the optimal value of the ground coverage ratio ( $x$ ) was found to be 0.57.

## 7. Analysis of the Optimized PV System

### 7.1. Analysis in Terms of Energy

The annual energy yield ( $EY$ ) is referred to as the ratio of energy generated by the system and the nominal power of the  $PV$  system [25] and is expressed as

$$EY = \frac{E_{PV}}{P_n} \quad (21)$$

where,  $P_n$  is the nominal power of the  $PV$  system. In the case of the roof-mounted  $PV$  system, the net energy yield of the optimized system is calculated by adding the cooling energy benefit of the roof-mounted  $PV$  system and is expressed as

$$Net - EY = \frac{E_{PV} + E_{sav}}{P_n} \quad (22)$$

The *Net-EY* of the optimized roof-mounted system was calculated to be 2919 kWh/kW. The *Net-EYs* of the roof-mounted  $PV$  system for different ground coverage ratio values are illustrated in Figure 7.

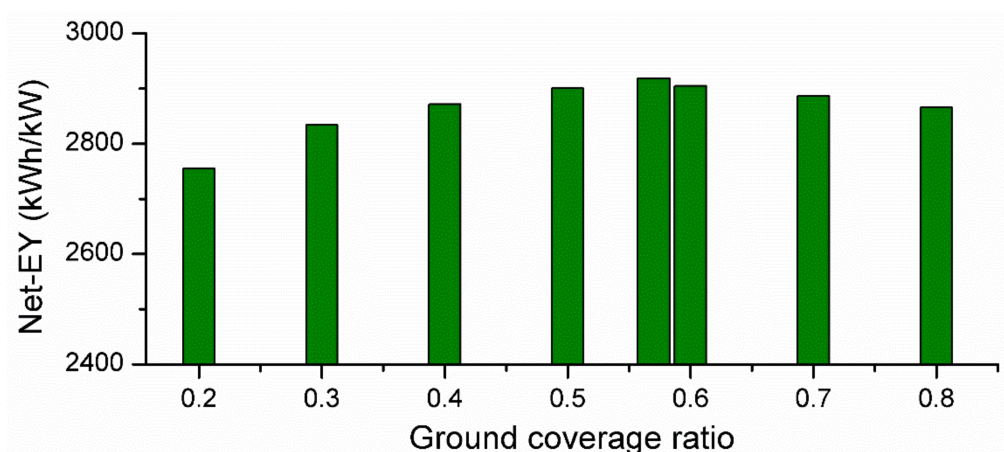


Figure 7. *Net-EY* of roof-mounted  $PV$  system at various ground coverage ratios.

The effectiveness of a PV project can be measured by another useful factor called performance ratio. It represents the ratio of PV real electrical output to its theoretical expected energy output and is given by the below expression [46].

$$\text{Performance ratio} = \frac{\text{PV electrical energy output}}{\text{GHI} \times \text{area of PV modules} \times \text{PV efficiency}} \quad (23)$$

The performance ratio of roof-mounted PV system can be calculated as

$$\text{Performance ratio} = \frac{\text{PV electrical energy output} + \text{cooling energy saving}}{\text{GHI} \times \text{area of PV modules} \times \text{PV efficiency}} \quad (24)$$

The performance ratios of roof-mounted PV system for different ground coverage ratio values are presented in Figure 8. The performance ratio of the optimized PV configuration was computed to be 1.19.

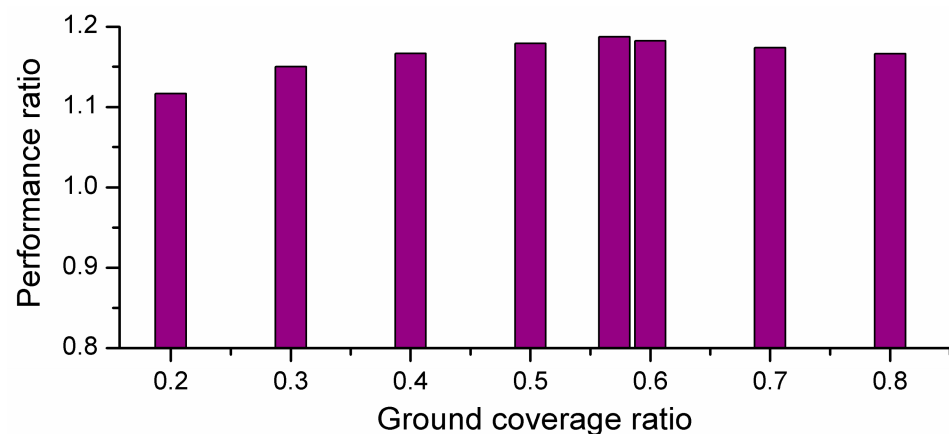


Figure 8. Performance ratio of roof-mounted PV system at various ground coverage ratios.

The Capacity Utilization Factor (CUF) of the PV system is expressed as (19) [47] while the Net-CUF of roof-mounted PV system also includes cooling energy savings as well and is expressed by Equation (20)

$$\text{CUF} = \frac{\text{electrical energy output}}{\text{nameplate capacity} \times 24 \times 365} \quad (25)$$

$$\text{Net-CUF} = \frac{\text{electrical energy output} + \text{cooling energy saving}}{\text{nameplate capacity} \times 24 \times 365} \quad (26)$$

The Net-CUFs of roof-mounted PV configuration for different ground coverage ratios are depicted in Figure 9. The optimized roof-mounted PV system has a Net-CUF of 33.3%.

It can be seen in Figures 7–9 that Net-EY, net performance ratio, and Net CUF of the roof-mounted PV are on the higher side for ground coverage ratios of 0.5 to 0.7 and the highest values of Net-EY, performance ratio and Net CUF are obtained at the optimal value of ground coverage ratio of 0.57 as found in Section 6. At low ground coverage ratio although the self-shading due to parallel arrays is less, more of the surface of the roof is exposed to direct sun rays which increases the cooling load requirement. On the other hand, higher values of ground coverage ratio, although protecting the roof outer surface from the direct contact of sun rays, mean that the self-shading of parallel PV arrays increases as a result of the output of the PV system declining. The optimal value of the ground coverage ratio of the PV systems gives a good compromise between roof shading to reduce the cooling energy requirement and self-shading to increase the PV system output.

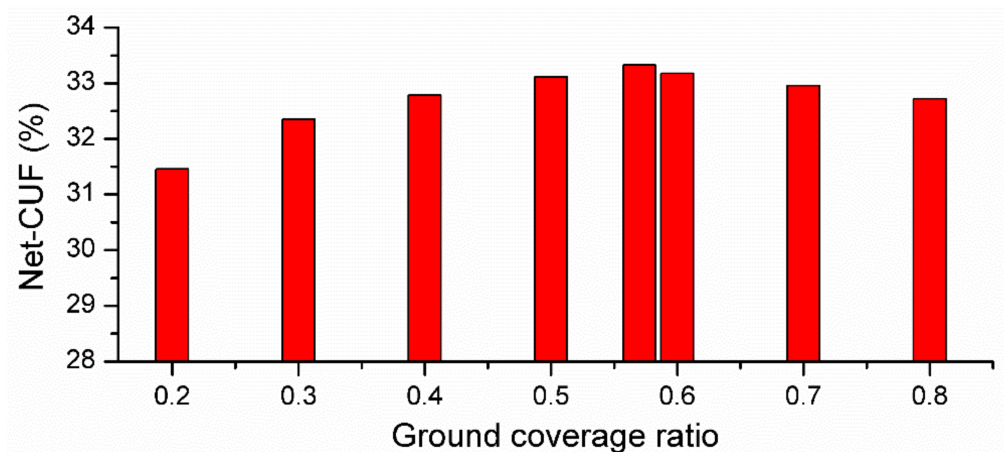


**Figure 9.** Net-CUF of roof-mounted PV system at various ground coverage ratios.

### 7.2. Economic Analysis

The economic feasibility of a renewable energy project can be tested by payback period and LCOE. The payback period of a project is represented by the time period required for refunding the capital cost along with possible interest that might be obtained by some alternative investment plan of the initial capital. The payback period and Net-LCOE of the roof-mounted PV system at various ground coverage ratios are illustrated in Figure 10. Both the payback period and Net-LCOE decrease with the increasing ground coverage ratio due to the decrease in cooling load energy requirement of the building. However, again, at the higher values of ground coverage ratio, such as while increasing the ground coverage ratio from 0.5 to 0.7, both payback period and Net-LCOE initially decrease but again at the ground coverage ratio of 0.7, there is a significant increase in payback period and Net-LCOE because the self-shading of the parallel PV arrays decreases the output of the PV system. The minimum values of payback period and Net-LCOE are achieved at the optimal ground coverage ratio of 0.57. The optimized roof-mounted PV system has a Net-LCOE of 3.21 c/kWh and its payback period is 2.82 years.

### 7.3. Comparative Analysis with Ground-Mounted PV System

In order to validate the proposed approach, the results of the optimized roof-mounted PV system are compared with the ground-mounted PV system. A land cost of 30,000 US\$/acre is considered for the analysis. The EY, performance ratio, CUF of the various configurations of the ground-mounted PV system are calculated by using (17), (19), and (21). The optimal ground coverage ratio value of the ground-mounted PV system with minimum LCoE is found to be 0.66 by using the same approach as in Section 6 but without the saving in the cooling energy term ( $E_{sav}$ ). The optimized configuration of the ground-mounted PV system has an EY of 2517 kWh/kW, CUF of 30.4%, performance ratio of 0.79, LCOE of 3.75, and payback period of 3.54 years. The comparison of the proposed optimized rooftop PV system and ground PV system is shown in Table 4.

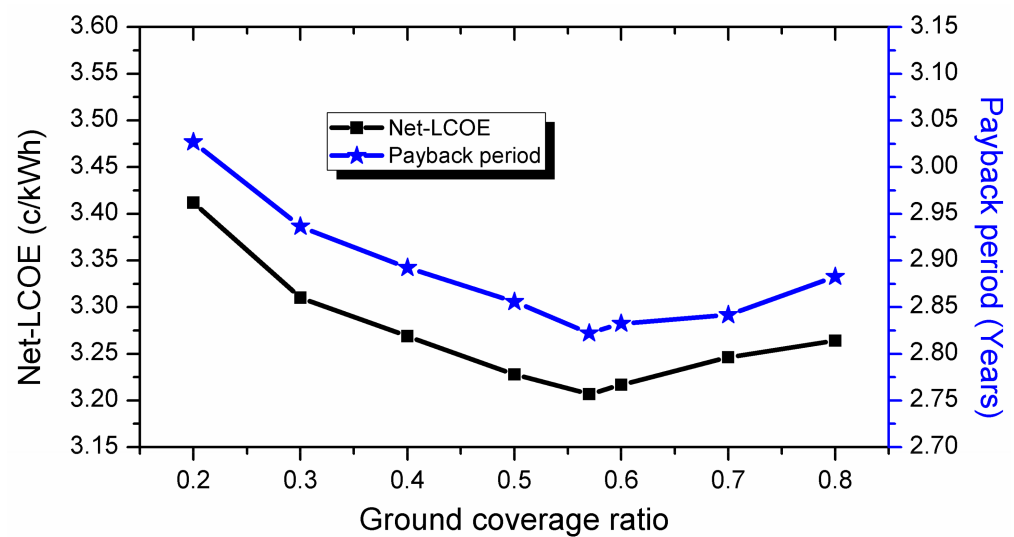


**Figure 10.** *Net-LCOE* and Payback period of roof-mounted *PV* system at various ground coverage ratios.

**Table 4.** Comparison of proposed optimized rooftop *PV* system with ground-mounted *PV* system.

Parameter	Rooftop <i>PV</i>	Ground Mounted
<i>EY</i>	2919 kWh/kW	2517 kWh/kW
<i>CUF</i>	33.3%	30.4%
Performance ratio	1.19	0.79
Payback period	2.82 year	3.54 year
<i>LCOE</i>	3.21 c/kWh	3.75 c/kWh

## 8. Conclusions

This research work investigated the possibility of using a roof-mounted *PV* system for the administration building of Majmaah University. The binate advantage of the roof-mounted *PV* system was explored, and the ground coverage ratio of the *PV* system optimized using the artificial neural network approach. Both the electrical energy output and shading advantage of the roof-mounted *PV* system were taken into account in the optimization of the ground coverage ratio. An energy function was formulated combining the *Net-LCOE* function and the ground coverage ratio constraint. This function was minimized using the artificial neural network approach. The network was converged after 20,000 cycles and at a ground coverage ratio of 0.57, the *Net-LCOE* was minimized. The concept of *Net-LCOE* and Net-energy yield was used while optimizing and analyzing the *PV* system. The Net-energy yield is the sum of the electrical energy output of the *PV* system and the cooling energy savings due to shading of the roof while the *Net-LCOE* is the *LCOE* calculated by adding the cooling energy saving and electrical energy output. A comparison of the proposed optimized roof-mounted *PV* system with the same size of ground-mounted *PV* system shows that the optimized roof-mounted *PV* system has a superior performance. The optimized roof-mounted *PV* system has 15.9% better energy yield, 2.9% better *CUF*, 20.3% shorter payback period, and 14.4% less *LCOE*. The results of this research work prove that roof-mounted *PV* is a very good option in hot climate regions from both the economical and the energy output point of view. This research work provides effective directions for future policy making to fulfil the energy demands of buildings in urban areas.

**Author Contributions:** The Conceptualization, methodology, data collection, analysis, writing of the manuscript is done by A.S.A. The author has read and agreed to the published version of the manuscript.

**Funding:** This research received no external funding.

**Institutional Review Board Statement:** Not applicable.

**Informed Consent Statement:** Not applicable.

**Data Availability Statement:** Not applicable.

**Conflicts of Interest:** The author declares no conflict of interest.

## Nomenclature

$A_{PV}$	PV array active area
$F_{PV}$	derating factor of PV
$X_{PV}$	PV output at STC
$G$	plane of array solar radiations
$G_{STC}$	solar radiation at STC
$T_{cell}$	PV cell temperature
$T_{cell\_STC}$	PV cell temperature at STC
$\alpha_p$	temperature coefficient of power
$q_{Roof}$	total heat flux into the roof
$q_{SW}$	shortwave solar radiations heat flux
$q_{LW}$	heat flux due to longwave radiations exchange
$q_{conv}$	convection heat flux
$T_r$	roof temperature
$T_a$	air temperature
$h_c$	convection coefficient
$\alpha_r$	surface albedo of roof
$Dif$	diffuse solar radiations
$q_{sky}$	heat fluxes due to exchange of radiation from sky
$q_{air}$	heat fluxes due to exchange of radiation from air
$\varepsilon$	emissivity
$\sigma$	Stefan–Boltzmann constant
$F_{sky}$	roof surface view factor to sky
$F_{air}$	roof surface view factor to air
$F_{PV}$	roof surface view factor
$T_{sky}$	sky temperature
$T_{PV\_b}$	PV back surface temperature
$C_{AN}$	annualized cost
$E_{PV}$	annual energy production of PV system
$n$	hour number
$P(n)$	electrical output of PV in hours $n$
$E_{sav}$	annual cooling energy saving
$C_{TPV}$	net present value of all costs
$r$	interest rate
$N$	project duration
$C_{Rep\_NPV}$	present value of equipment replacement cost
$C_{O\&M\_NPV}$	present value of operation and maintenance cost
$C_{G\_NPV}$	present worth of cooling load saving
$P_n$	nominal power of the PV system
$I_i$	input to the $i^{th}$ node of input layer
$E$	energy function
$\nabla_E$	gradient of the energy function
$\eta$	learning rate
$O_j$	output at the $i^{th}$ node of output layer
$F(X)$	objective function to be minimized
$K$	penalty constant
$P[r_i(X)]$	penalty function
$r^2$	residual of the constraint violation

### Abbreviations

ABMU	administration building of Majmaah University
CRF	capital recovery factor
CC	capital cost
CUF	capacity utilization factor
DHI	diffuse horizontal irradiance
EY	energy yield
LCOE	levelized cost of energy
GHI	global horizontal irradiance
GHG	greenhouse gas
PV	photovoltaic
STC	standard test condition

### References

- Bocquier, P. World Urbanization Prospects: An alternative to the UN model of projection compatible with the mobility transition theory. *Demogr. Res.* **2005**, *19*, 197–236. [CrossRef]
- Pérez-Lombard, L.; Ortiz, J.; Pout, C. A review on buildings energy consumption information. *Energy Build.* **2008**, *40*, 394–398. [CrossRef]
- Diraco, G.; Leone, A.; Siciliano, P. People occupancy detection and profiling with 3D depth sensors for building energy management. *Energy Build.* **2015**, *92*, 246–266. [CrossRef]
- Deng, S.; Wang, R.Z.; Dai, Y.J. How to evaluate performance of net zero energy building—A literature research. *Energy* **2014**, *71*, 1–16. [CrossRef]
- European Parliament. Directive No. 2009/28/EC of the European Parliament and of the Council of 23 April 2009, on the Promotion of the Use of Energy from Renewable Sources and Amending and Subsequently Repealing Directives No. 2001/77/EC and No. 2003/30/EC. *Off. J. Eur. Union* **2009**, *2009*, 5.
- Machete, R.; Paula, A. The use of 3D GIS to analyse the influence of urban context on buildings' solar energy potential. *Energy Build.* **2018**, *177*, 290–302. [CrossRef]
- Asif, M. Growth and sustainability trends in the buildings sector in the GCC region with particular reference to the KSA and UAE. *Renew. Sustain. Energy Rev.* **2016**, *55*, 1267–1273. [CrossRef]
- Government of Saudi Arabia. A Renewable Energy Market, Saudi Arabia Vision 2030. Available online: <http://vision2030.gov.sa/en/node/87> (accessed on 10 December 2018).
- Abdelhafez, M.H.H.; Touahmia, M.; Noaime, E.; Albaqawy, G.A.; Elkhayat, K.; Achour, B.; Boukendakdji, M. Integrating Solar Photovoltaics in Residential Buildings: Towards Zero Energy Buildings in Hail City, KSA. *Sustainability* **2021**, *13*, 1845. [CrossRef]
- Lucchi, E.; Polo Lopez, C.S.; Franco, G. A conceptual framework on the integration of solar energy systems in heritage sites and buildings. *IOP Conf. Ser. Mater. Sci. Eng.* **2020**, *949*. [CrossRef]
- Zubair, M.; Awan, A.B.; Rp, P. Analysis of photovoltaic arrays efficiency for reduction of building cooling load in hot climates. *Build. Serv. Eng. Res. Technol.* **2018**, *39*, 733–748. [CrossRef]
- Zubair, M.; Awan, A.B.; Abo-khalil, A.G. NPC Based Design Optimization for a Net Zero Office Building in Hot Climates with PV Panels as Shading Device. *Energies* **2018**, *11*, 1391. [CrossRef]
- Wu, P.; Ma, X.; Ji, J.; Ma, Y. Review on life cycle assessment of energy payback of solar photovoltaic systems and a case study. *Energy Procedia* **2017**, *105*, 68–74. [CrossRef]
- Peng, J.; Lu, L. Investigation on the development potential of rooftop PV system in Hong Kong and its environmental benefits. *Renew. Sustain. Energy Rev.* **2013**, *27*, 149–162. [CrossRef]
- Bhatti, A.R.; Salam, Z.; Sultana, B.; Rasheed, N.; Awan, A.B.; Sultana, U.; Younas, M. Optimized sizing of photovoltaic grid-connected electric vehicle charging system using particle swarm optimization. *Int. J. Energy Res.* **2019**, *43*, 500–522. [CrossRef]
- Afzaal, M.U.; Sajjad, I.A.; Awan, A.B.; Paracha, K.N.; Khan, M.F.N.; Bhatti, A.R.; Zubair, M.; Rehman, W.U.; Amin, S.; Haroon, S.S.; et al. Probabilistic generation model of solar irradiance for grid connected photovoltaic systems using weibull distribution. *Sustainability* **2020**, *12*, 2241. [CrossRef]
- Suárez-García, A.; Fariña, E.A.; Álvarez-Feijoo, M.; González-Peña, D.; Alonso-Tristán, C.; Díez-Mediavilla, M. Estimation of photovoltaic potential for electricity self-sufficiency: A study case of military facilities in northwest Spain. *J. Renew. Sustain. Energy* **2017**, *9*, 053503. [CrossRef]
- Zubair, M.; Awan, A.B.; Praveen, R.P.; Abdulbaseer, M. Solar energy export prospects of the Kingdom of Saudi Arabia. *J. Renew. Sustain. Energy* **2019**, *11*, 045902. [CrossRef]
- Zubair, M.; Ghuffar, S.; Shoaib, M.; Bilal Awan, A.; Bhatti, A.R. Assessment of PV Capabilities in Urban Environments, Case study of Islamabad, Pakistan. *J. Sol. Energy Eng.* **2020**, *142*, 1–24. [CrossRef]
- Kotak, Y.; Gago, E.J.; Mohanty, P.; Muneer, T. Installation of roof-top solar PV modules and their impact on building cooling load. *Build. Serv. Eng. Res. Technol.* **2014**, *35*, 613–633. [CrossRef]
- Ban-weiss, G.; Wray, C.; Delp, W.; Ly, P.; Akbari, H.; Levinson, R. Electricity production and cooling energy savings from installation of a building-integrated photovoltaic roof on an office building. *Energy Build.* **2013**, *56*, 210–220. [CrossRef]

22. ĀIqbal, I.; Al-homoud, M.S. Parametric analysis of alternative energy conservation measures in an office building in hot and humid climate. *Build. Environ.* **2007**, *42*, 2166–2177. [[CrossRef](#)]
23. Huang, L.; Zheng, R. Energy and Economic Performance of Solar Cooling Systems in the Hot-Summer and Cold-Winter Zone. *Buildings* **2018**, *8*, 37. [[CrossRef](#)]
24. Ramli, M.A.M.; Twaha, S.; Alghamdi, A.U. Energy production potential and economic viability of grid-connected wind/PV systems at Saudi Arabian coastal areas. *J. Renew. Sustain. Energy* **2017**, *9*, 065910. [[CrossRef](#)]
25. Awan, A.; Zubair, M.; Abokhalil, A. Solar Energy Resource Analysis and Evaluation of Photovoltaic System Performance in Various Regions of Saudi Arabia. *Sustainability* **2018**, *10*, 1129. [[CrossRef](#)]
26. Prieto, A.; Knaack, U.; Auer, T.; Klein, T. Passive cooling & climate responsive façade design Exploring the limits of passive cooling strategies to improve the performance of commercial buildings in warm climates. *Energy Build.* **2018**, *175*, 30–47. [[CrossRef](#)]
27. Cronemberger, J.; Caama, E.; Vega, S. Assessing the solar irradiation potential for solar photovoltaic applications in buildings at low latitudes—Making the case for Brazil. *Energy Build.* **2012**, *55*, 264–272. [[CrossRef](#)]
28. Mandalaki, M.; Papantoniou, S.; Tsoutsos, T. Assessment of energy production from photovoltaic modules integrated in typical shading devices. *Sustain. Cities Soc.* **2014**, *10*, 222–231. [[CrossRef](#)]
29. Mandalaki, M.; Zervas, K.; Tsoutsos, T.; Vazakas, A. Assessment of fixed shading devices with integrated PV for efficient energy use. *Sol. Energy* **2012**, *86*, 2561–2575. [[CrossRef](#)]
30. Assouline, D.; Mohajeri, N.; Scartezzini, J. Large-scale rooftop solar photovoltaic technical potential estimation using Random Forests. *Appl. Energy* **2018**, *217*, 189–211. [[CrossRef](#)]
31. Yadav, S.K.; Bajpai, U. Performance evaluation of a rooftop solar photovoltaic power plant in Northern India. *Energy Sustain. Dev.* **2018**, *43*, 130–138. [[CrossRef](#)]
32. Kumar, N.M.; Gupta, R.P.; Mathew, M.; Jayakumar, A.; Singh, N.K. Performance, energy loss, and degradation prediction of roof-integrated crystalline solar PV system installed in Northern India. *Case Stud. Therm. Eng.* **2019**, *13*, 1–9. [[CrossRef](#)]
33. Shukla, A.K.; Sudhakar, K.; Baredar, P. Design, simulation and economic analysis of standalone roof top solar PV system in India. *Sol. Energy* **2016**, *136*, 437–449. [[CrossRef](#)]
34. Awan, A.B.; Alghassab, M.; Zubair, M.; Bhatti, A.R.; Uzair, M.; Abbas, G. Comparative Analysis of Ground-Mounted vs. Rooftop Photovoltaic Systems Optimized for Interrow Distance between Parallel Arrays. *Energies* **2020**, *13*, 3639. [[CrossRef](#)]
35. Dondariya, C.; Porwal, D.; Awasthi, A.; Shukla, A.K.; Sudhakar, K.; Murali, M.M.; Bhimte, A. Performance simulation of grid-connected rooftop solar PV system for small households: A case study of Ujjain, India. *Energy Rep.* **2018**, *4*, 546–553. [[CrossRef](#)]
36. Akpolat, A.N.; Dursun, E.; Kuzucuoğlu, A.E.; Yang, Y.; Blaabjerg, F.; Baba, A.F. Performance analysis of a Grid-connected rooftop solar photovoltaic system. *Electronics* **2019**, *8*, 905. [[CrossRef](#)]
37. Said, S.A.M. Effects of dust accumulation on performances of thermal and photovoltaic flat-plate collectors. *Appl. Energy* **1990**, *37*, 73–84. [[CrossRef](#)]
38. Baras, A.; Jones, R.K.; Alqahtani, A.; Alodan, M.; Abdullah, K. Measured soiling loss and its economic impact for PV plants in central Saudi Arabia. In Proceedings of the 2016 Saudi Arabia Smart Grid (SASG), Jeddah, Saudi Arabia, 6–8 December 2016; pp. 1–7.
39. Awan, A.B. Optimization and techno-economic assessment of rooftop photovoltaic system. *J. Renew. Sustain. Energy* **2019**, *11*. [[CrossRef](#)]
40. NREL EnergyPlus Engineering Reference. Available online: [https://energyplus.net/sites/all/modules/custom/nrel\\_custom/pdfs/pdfs\\_v8.9.0/EngineeringReference.pdf](https://energyplus.net/sites/all/modules/custom/nrel_custom/pdfs/pdfs_v8.9.0/EngineeringReference.pdf) (accessed on 5 June 2020).
41. Awan, A.B.; Bhatti, A.R.; Zubair, M.; Khalil, A.G.A.; Ahmed, G.; Sidhu, S. Performance analysis of various hybrid renewable energy systems using battery, hydrogen, and pumped hydro-based storage units. *Int. J. Energy Res.* **2019**, *43*, 6296–6321. [[CrossRef](#)]
42. Lazou, A.A.; Papatsoris, A.D. Economics of photovoltaic stand-alone residential households: A case study for various European and Mediterranean locations. *Sol. Energy Mater. Sol. Cells* **2000**, *62*, 411–427. [[CrossRef](#)]
43. Maleki, A.; Ameri, M.; Keynia, F. Scrutiny of multifarious particle swarm optimization for finding the optimal size of a PV/wind/battery hybrid system. *Renew. Energy* **2015**, *80*, 552–563. [[CrossRef](#)]
44. Saudi Electricity Company. Available online: <https://www.se.com.sa/en-us/customers/Pages/TariffRates.aspx> (accessed on 28 February 2021).
45. Awan, A.B.; Zubair, M.; Chandra Mouli, K.V.V. Design, optimization and performance comparison of solar tower and photovoltaic power plants. *Energy* **2020**, *199*, 117450. [[CrossRef](#)]
46. Sharma, V.; Kumar, A.; Sastry, O.S.; Chandel, S.S. Performance assessment of different solar photovoltaic technologies under similar outdoor conditions. *Energy* **2013**, *58*, 511–518. [[CrossRef](#)]
47. Awan, A.B.; Zubair, M.; Praveen, R.P.; Bhatti, A.R. Design and comparative analysis of photovoltaic and parabolic trough based CSP plants. *Sol. Energy* **2019**, *183*, 551–565. [[CrossRef](#)]